# A SRS2 homolog from *Arabidopsis thaliana* disrupts recombinogenic DNA intermediates and facilitates single strand annealing

Sandra Blanck, Daniela Kobbe, Frank Hartung, Karin Fengler, Manfred Focke and Holger Puchta*

Botanical Institute II, Karlsruhe Institute of Technology (KIT), Kaiserstr. 12, 76128 Karlsruhe, Germany

## ABSTRACT

**Genetic and biochemical analyses of SRS2 homologs in fungi indicate a function in the processing of homologous recombination (HR) intermediates. To date, no SRS2 homologs have been described and analyzed in higher eukaryotes. Here, we report the first biochemical characterization of an SRS2 homolog from a multicellular eukaryote, the plant *Arabidopsis thaliana*. We studied the basic properties of AtSRS2 and were able to show that it is a functional 3′- to 5′-helicase. Furthermore, we characterized its biochemical function on recombinogenic intermediates and were able to show the unwinding of nicked Holliday junctions (HJs) and partial HJs (PX junctions). For the first time, we demonstrated strand annealing activity for an SRS2 homolog and characterized its strand pairing activity in detail. Our results indicate that AtSRS2 has properties that enable it to be involved in different steps during the processing of recombination intermediates. On the one hand, it could be involved in the unwinding of an elongating invading strand from a donor strand, while on the other hand, it could be involved in the annealing of the elongated strand at a later step.**

## INTRODUCTION

Helicases are enzymes that modulate the structure of nucleic acids. To disrupt the hydrogen bonds of dsDNA, the helicases utilize the free energy of the hydrolysis of nucleoside triphosphates. These motor proteins are known to play a role in almost every aspect of nucleic acid metabolism, including DNA replication, recombination, transcription and repair. Helicases consist of conserved helicase motifs, and they are classified by the homology and organization of those motifs (1–3).

We are interested in the mechanism of DNA repair and homologous recombination (HR) in plants, using the model organism *Arabidopsis thaliana* (4,5). In this study, we focus on the biology of the plant DNA helicase AtSRS2 and its possible role in DNA repair by HR. The yeast SRS2 helicase (Suppressor of RAD Six-screen mutant 2) belongs to the SF1 family of helicases and shows structural und functional similarities to the bacterial helicases UVRD, REP and PCRA (6,7).

*SRS2* was first recognized as a mutant variant in *Saccharomyces cerevisiae* that suppressed the repair defects of *rad6* and *rad18* mutants, which were defective in the postreplicative DNA repair (PRR) pathway (8). Further studies showed a hyper-recombination phenotype of *srs2* strains (6,8,9). Additionally, it was demonstrated that posttranslational modification of PCNA recruits SRS2 to stalled replication forks (10,11). In accordance with these data, genetic analyses also revealed that SRS2 regulates the RAD52-mediated HR in a negative way and that SRS2 removes toxic recombination intermediates (9,12–16). Taken together, these genetic data indicate that SRS2 can function on stalled replication forks, ensuring that recombination events do not occur or are repaired by the PRR pathway.

Several genetic studies indicate that SRS2 also plays a role in DSB repair by HR (17–19). Moreover, *in vitro* studies support the hypothesis that SRS2 acts as an antirecombinase. It was shown that SRS2 prevents recombination by disrupting the RAD51 presynaptic filament (20,21). Early *in vitro* studies focused on the analyses of the helicase activity of SRS2 on relatively simple DNA substrates (22,23). Recently, the question of the biological function of the SRS2 displacement activity arose, and therefore Dupaigne *et al.* (24) investigated the helicase activity on recombination intermediates that occur during HR. They found that SRS2 is indeed able to disrupt recombination intermediates and is even able to

*To whom correspondence should be addressed. Tel: +49 721 608 8894; Fax: +49 608 4874; Email: holger.puchta@bio.uka.de

translocate along RPA coated ssDNA and that the helicase activity is stimulated by RAD51 nucleoprotein filaments. These data strongly support the hypothesis that SRS2 promotes synthesis-dependent strand annealing (SDSA), thus preventing crossover events, and, moreover, they show that the strand displacement activity of SRS2 could play a role in disrupting the recombination intermediates emerging during SDSA.

The SRS2 helicase is conserved in other fungi like *Schizosaccharomyces pombe* and *Neurospora crassa*, but no other SRS2 homologs have been described in other eukaryotes until now (25–28). Although it is indicated that the human FBH1 helicase is functionally related to the yeast SRS2 protein, no sequence homolog has been found thus far (29,30).

Here, we present the first biochemical study of an SRS2 homolog from a multicellular eukaryote, the AtSRS2 helicase from the model plant *A. thaliana*. We were able to demonstrate that the recombinant AtSRS2 protein is a functional DNA helicase with 3′- to 5′-directionality. AtSRS2 is also able to process branched structures that occur during SDSA, indicating that AtSRS2 might play a role in HR as predicted for ScSRS2 (24). Moreover, we were able to detect a new feature that has not yet been described for SRS2, namely, AtSRS2-dependent strand pairing. We conclude that the AtSRS2-dependent strand pairing activity could play a role in the re-annealing of the displaced elongated strand during SDSA.

## MATERIALS AND METHODS

### RNA extraction, RT-PCR and RACE of AtSRS2

RNA from young Arabidopsis plantlets was isolated using the RNeasy Plant Mini Kit from Qiagen (Hilden, Germany) according to the instructions of the manufacturer. Reverse transcription and RT-PCR were performed according to the SMART protocol from Clontech (Heidelberg, Germany) using 50–100 ng of mRNA. The 5′- and 3′-rapid amplification of cDNA ends (RACE) was performed according to Matz *et al.* (31). The produced cDNA fragments were sequenced and aligned to the genomic database of TAIR (The Arabidopsis Information Resource). The full-length cDNA was submitted in the database Genbank (acc. no. GQ148553).

### Bioinformatic methods

Assembly of the sequenced cDNA, pairwise alignment and ClustalW alignments of the protein sequences from AtSRS2 and all other protein sequences were performed with the DNAstar package from Lasergene.

### Cloning, expression and purification of AtSRS2 and AtSRS2-K273R

AtSRS2 and AtSRS2-K273R were cloned according to the procedure as described by Kobbe *et al.* (32,33). AtSRS2-K273R is bearing a point mutation K273R in the Walker A motif of the conserved ATPase domain, as for example in Krejci *et al.* (34).

Expression and purification of AtSRS2 and AtSRS2-K273R were carried out similar to the procedure as described earlier (32,33) with the exception that the expression of both proteins were carried out at 16°C for 6 h, and the purification was also slightly modified. Buffer A consisted of 50 mM $NaH_2PO_4$, 200 mM NaCl, 10 mM imidazole, 10% glycerol, 5 mM 3–mercapto-1, 2-propanediol (thioglycerol), pH 8.0 and buffer B (buffer A with 400 mM imidazole). Contaminant proteins were removed for 15 min at 13% buffer B, and AtSRS2 and AtSRS2-K273R were eluted with 100% of buffer B for 15 min. After exchanging the buffer with buffer C [50 mM Tris, 500 mM NaCl, 2 mM $CaCl_2$, 1 mM $Mg(CH_3COO)_2$, 1 mM imidazole, 5 mM thioglycerol, pH 8.0], the eluate was directly applied on 1 ml of equilibrated calmodulin (CaM) affinity resin (Stratagene), followed by several washing steps (3 ml buffer C, then 3 ml buffer C with 0.5% Triton X-100 and 3 ml buffer C) and the protein was eluted with buffer D (50 mM Tris, 500 mM NaCl, 2 mM EGTA, 5 mM thioglycerol). The eluate was mixed with the same volume of glycerol, and aliquots of the purified proteins were stored at −80°C. The proteins were quantified on colloidal Coomassie-stained SDS–PAGE gels using BSA (Bio-Rad) as a standard.

### DNA substrates and oligonucleotides

All oligonucleotides used in this study were purchased from Biomers. Respective oligonucleotides were 5′-end-labeled with [γ-$^{32}$P]ATP from GE Healthcare or Hartmann Analytics using T4 polynucleotide kinase from New England Biolabs. Excess of [γ-$^{32}$P]ATP was removed by gel filtration (G25microSpin, GE Healthcare).

To study the basic properties of the helicase activity of AtSRS2, we used an M13mp18ssDNA based substrate that was prepared as described earlier (32). The sequences and construction of the DNA substrates for determining the directionality and required length of the 3′-overhang were taken from van Komen *et al.* (23). Oligonucleotides used for the formation of the branched substrates X0-HJ, X0-nHJ and the PX junction (31-bp duplex region) were designed as described by Dupaigne *et al.* (24). The partially mobile HJ X12-HJ consisting of an homologous core of 12-bp flanked by arms of 19 bp was designed as described by Mohaghegh *et al.* (35) and the static HJ (24-bp duplex region) were used as by Boddy *et al.* and Gaillard *et al.* (36,37). Annealing reactions of the branched substrates were carried out at 95°C for 5 min and cooling down to room temperature over ~3 h using a molar ratio of 1:4 labeled to non-labeled oligonucleotide. The branched structures were purified by gelextraction in TB-$MgCl_2$ buffer (44.5 mM Tris–Base, 44.5 mM boric acid and 5 mM $MgCl_2$) using D-Tube$^{TM}$ Dialyzers (Merck).

Labeled and purified oligonucleotides with sequences taken from van Komen *et al.* (23), were used for studying the annealing reactions of AtSRS2 and AtSRS2-K273R. To determine the minimal duplex length of the annealing activity, we designed additional oligonucleotides. Based on the 40-nt H1 and 80-nt H4 oligonucleotides of van Komen *et al.* (23), we designed

sequences that were shortened 5, 10, 15, 20 and 25 nt in the duplex region.

### Helicase assays

The studying of the strand displacement activity of AtSRS2 was in general carried out at 30°C with 150 pM of labeled DNA substrate in helicase reaction buffer [40 mM Tris acetate (pH 8.0), 50 mM potassium acetate, 6 mM DTT, 50 μg ml$^{-1}$ BSA, 1.8 mM ATP and 1.8 mM or 5.4 mM MgCl$_2$], and indicated amounts of AtSRS2 in a total reaction volume of 20 μl. Usually, the reactions were started by addition of the reaction buffer and substrate to the enzyme, incubated at 30°C and stopped after 10 or 20 min by addition of 3× termination buffer (50 mM EDTA, 0.6% SDS, 0.1% xylene cyanol, 0.1% bromophenol blue and 20% glycerol). In order to analyze the time-dependent helicase activity, aliquots were removed at the indicated time points and added to the termination buffer.

The reaction products were separated by electrophoresis on native polyacrylamide gels in Tris–Borate–EDTA (TBE) buffer at 4°C. After gelelectrophoresis, the gels were either dried or immediately analyzed using the Instant Imager (Canberra Packard) or BIO-Image analyzer BAS-1500. The ratio of separated DNA to non-separated DNA was calculated as by Mohaghegh *et al.* (35) from the formula:

Percent displacement

$$= \left[ \frac{(\text{percent product} - \text{percent product}_{-\text{enzyme}})}{(\text{percent product}_{\text{denatured}} - \text{percent product}_{-\text{enzyme}})} \right] \times 100$$

The error bars were calculated using the standard deviation.

### Annealing assay

Annealing reactions were performed under the same conditions as for the helicase assay, except using 5.4 mM MgCl$_2$ exclusively in the reaction buffer. The reactions were started by mixing the reaction buffer containing 150 pM labeled oligonucleotide with indicated amounts of AtSRS2 or AtSRS2-K273R followed by addition of 150 pM complementary non-labeled oligonucleotide. After incubation at 30°C for 20 min, the reactions were stopped as described for the helicase assay, and quantified according to the formula:

Percent annealing

$$= \left[ \frac{(\text{percent product} - \text{percent product}_{-\text{enzyme}})}{(\text{percent product}_{\text{annealed}} - \text{percent product}_{-\text{enzyme}})} \right] \times 100$$

The calculation of the error bars were done as mentioned above.

## RESULTS

### Identification of an SRS2 homolog in *A. thaliana*: AtSRS2

By performing a BLAST-search with the yeast SRS2 protein sequence, we were able to identify only one candidate gene homolog in *Arabidopsis*, which is located on chromosome 4 (At4g25120). Our RT-PCR and RACE analyses of this gene, named AtSRS2, demonstrated that it codes for a cDNA of 3664 nt. This full-length cDNA sequence includes a 56-nt 5′-UTR and 164-nt 3′-UTR. The protein encoded by this cDNA is 1147 amino acids long and differs from the predicted sequence of At4g25120 by three exons. The total gene consists of 29 exons, spanning a region of 7835 bp. Exon 5 is 19 amino acid longer in its 3′-region, and exon 24 is 8 amino acid shorter in its 5′-region, than predicted. Additionally, exon 3 was not at all depicted in the database prediction of At4g25120. In total, the suggested coding sequence is 25 amino acid shorter than the ORF encoded by the cDNA found in our analyses.

Using the full-length protein sequence of AtSRS2, we aligned it pairwise to the known yeast sequences of *S. cerevisiae* and *S. pombe*. Against both yeast protein sequences, AtSRS2 exhibits a sequence identity of 22 and 22.5%, respectively, ranging from amino acid 241–1141 of the entire protein, which is 1147 amino acid long. The conserved UVRD/REP domain of the proteins could be clearly aligned and shows that At4g25120 is really homologous to SRS2. When comparing only the UVRD domain, the identity between AtSRS2 and SpSRS2 or ScSRS2 is 24.2 and 23.8%, respectively (Figure 1). To strengthen the hypothesis that At4g25120 is a true and conserved SRS2 homolog, we analyzed the conservation of SRS2 throughout the plant kingdom, using already sequenced genomes of various plants at the JGI (Joint Genome Institute) server and the protein sequence of AtSRS2. In all investigated land plants, an unambiguous homolog of AtSRS2 is present. The identity between the different plants varies in the range of 40–65%, depending on their phylogenetic distances (e.g. as highest distance from *A. thaliana* to *Physcomitrella patens* 40% and 65.9% between *Arabidopsis* and *Ricinus communis*). Furthermore, we could also detect SRS2 homologs in other Viridiplantae like green- and microalgae (e.g. *Chlamydomonas reinhardtii* and *Volvox carteri*), the Prasinophyceae (e.g. *Ostreococcus lucimarinus*), and in the two Heterokonts, *Thalassiosira pseudonana* and *Phaeodactylum tricornutum*. The SRS2 proteins found in these more ancient organisms are less conserved, but all range from 20% to 35% identity with AtSRS2. Expanding our bioinformatic analyses into the animal kingdom, for which no SRS2 homolog has been reported so far, we found segments of sequences showing a reasonable homology to all three UVRD/REP helicase domains of SRS2. In all organisms up to the amphibia, SRS2 homologs are present in the genome. For example we detected SRS2 genes in cnidaria (*Hydra magnipapillata*), nematodes (*C. elegans*), insects (*Aedes aegyptii*), lower chordata (*Ciona intestinalis*) and amphibia (*Xenopus tropicalis*), but not in bony fishes (*Takifugu rubripes*, *Danio rerio*) or mammals (*Homo sapiens*, *Mus musculus*). In summary, a clearly definable SRS2 homolog exists as a single copy gene throughout all members of the Viridiplantae, Heterokonts and Metazoa except fish and mammals investigated thus far.
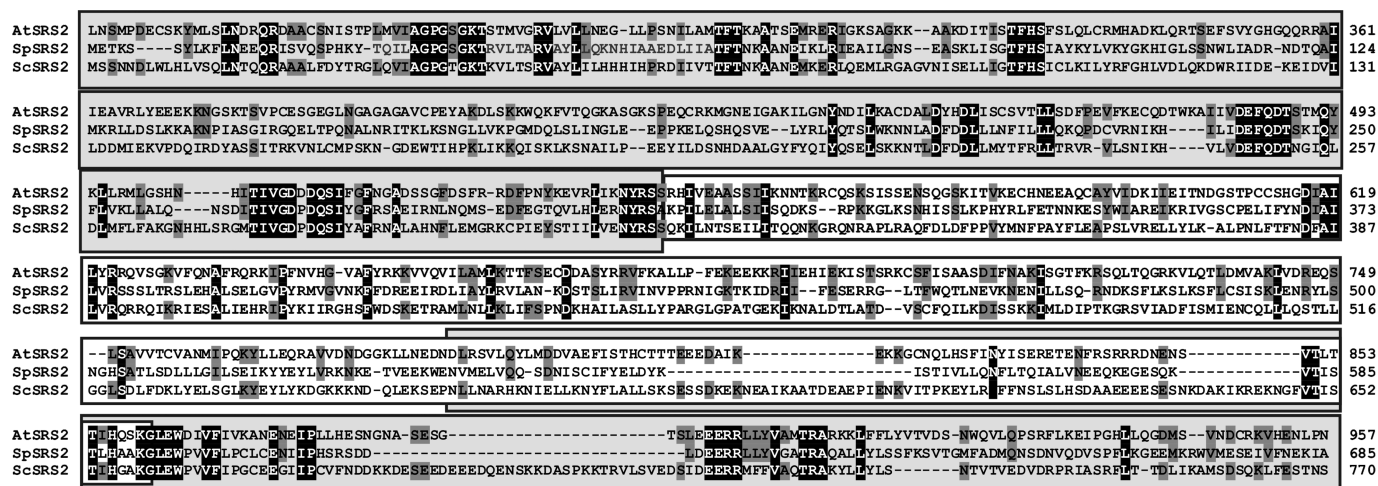
**Figure 1.** ClustalW alignment of the SRS2 UVRD-domain from Arabidopsis and yeasts. The UVRD domain of AtSRS2 is shown in a ClustalW alignment to SRS2 of *S. cerevisiae* and *S. pombe*. According to the InterProScan tool (http://www.ebi.ac.uk/Tools/InterProScan/), the sequence of the UVRD-domain ranges from amino acid 246 to 957 from AtSRS2 and contains three Interpro motifs. IPR014016 (superfamily 1, UVRD related, first gray shaded box) ranges from amino acid 246 to 548, IPR014017 (UVRD-like, C-terminal, white box) from a 549 to 860 and IPR000212 (DNA helicase UVRD/REP type, second gray shaded box) from amino acid 785–957. IPR014017 and 000212 show an overlap of 76 amino acids. Amino acids identical in all three sequences are shaded in black using white letters, amino acids identical between *Arabidopsis* and at least one of the two yeast sequences are shaded in gray. The name of the respective protein is shown in the first lines of each sequence on the left and the numbering for each line on the right. At, *Arabidopsis thaliana*; Sp, *Schizosaccharomyces pombe*; Sc, *Saccharomyces cerevisiae*.

Thus, SRS2 must have been lost only during the development of the taxa Teleostei and mammalia.

## AtSRS2 is a functional DNA helicase

We expressed AtSRS2 in *Escherichia coli* and purified the recombinant protein using two affinity tags. The purified proteins exhibit the expected size on a colloidal Coomassie-stained SDS–PAGE gel (Supplementary Figure S1). Using antibodies directed against the N-terminal FLAG tag and the C-terminal His tag, it was demonstrated that the proteins were not degraded either N- or C-terminally (data not shown). We tested the strand displacement activity of the recombinant AtSRS2 on an M13mp18ssDNA-based DNA substrate providing both 3′- and 5′-flaps. The recombinant AtSRS2 is able to separate the oligonucleotide from the circular M13ssDNA in a concentration-dependent manner (Figure 2A). Furthermore, the reaction is dependent on ATP, and no displacement is obtained without AtSRS2 in the reaction. No strand displacement activity is displayed by comparable preparations of AtSRS2-K273R, which is an ATPase-deficient variant of the AtSRS2 protein due to an amino acid substitution in the conserved Walker A motif. Thus, the recombinant AtSRS2 is a functional DNA helicase, and its preparation is suitable for the biochemical characterization.

## General characteristics of AtSRS2

In order to find the optimal reaction conditions for the strand displacement activity of AtSRS2, we tested different reaction conditions for the disruption of the M13-based substrate. We observed strand displacement activity at a broad pH range in Tris–acetate buffer and various concentrations of potassium–acetate (data not shown). The optimal reaction conditions were at pH 8 with 50 mM potassium acetate.

We also tested the temperature dependence of AtSRS2 in order to define the optimal incubation temperature. No significant differences in the disruption of different DNA substrates were observed at temperatures between 22°C and 37°C. Furthermore, we could still observe helicase activity at 4°C (data not shown). Further experiments were carried out at 30°C, which corresponds to the incubation temperature of ScSRS2 (23).

To classify AtSRS2 in terms of its directionality, we used three different DNA substrates that consisted of a 40-bp duplex region with either a 40-nt 5′-overhang, a 40-nt 3′-overhang or no overhang. Under standard reaction conditions, AtSRS2 separated the 3′-overhang DNA substrates, but not the 5′-overhang or blunt-end substrates (Figure 2B and C). We addressed the question of whether the 5′-overhang and blunt-end substrates were unwound under different reaction conditions. Thus, we modified the incubation temperature or the amount of DNA substrate and enzyme (data not shown). However, we did not observe separation of the 5′-overhang and the blunt-end substrate in any case. We also tested three different DNA substrates with shorter duplex regions (15 bp), but AtSRS2 only displaced the oligonucleotide from the 3′-overhang substrate (data not shown). Hence, we classify AtSRS2 as a 3′- to 5′-DNA helicase.

We further examined the strand displacement activity of AtSRS2 with different divalent cations. As Figure 3A and B illustrate, $Mg^{2+}$ can be replaced by $Mn^{2+}$, whereas little strand displacement is seen with $Ca^{2+}$ and no helicase activity can be observed with $Zn^{2+}$. We additionally showed that ATP could be replaced by dATP, but not by (d)GTP, (d)CTP, UTP or dTTP (Figure 3C).
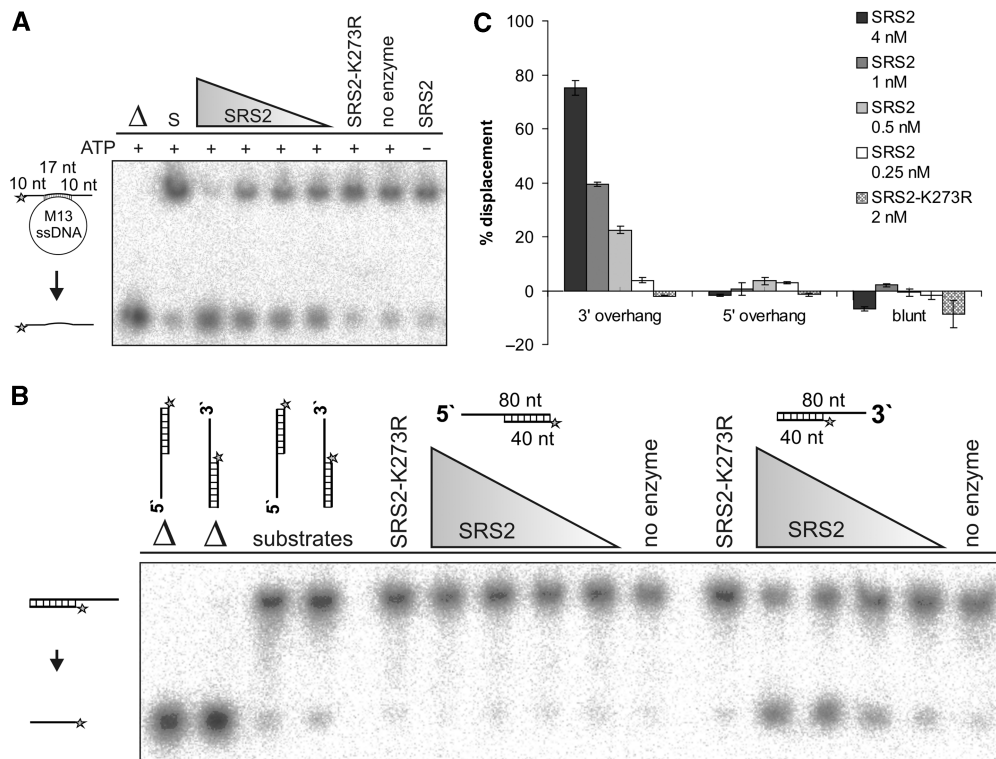
**Figure 2.** Demonstration of the helicase activity and directionality of AtSRS2. (**A**) The M13-based substrate and the separated, labeled (asterisk) oligonucleotide is drafted on the left. Decreasing concentrations of AtSRS2 (8, 3, 2 and 1.5 nM AtSRS2) and 2 nM AtSRS2-K273R were analyzed. Δ marks the heat-denatured M13-based substrate, S the entire M13-based substrate. The reaction was carried out as described in 'Materials and Methods' section using 1.8 mM ATP and 1.8 mM MgCl$_2$. The reaction products were separated by 12% TBE–PAGE. (**B** and **C**) Directionality of AtSRS2. (**B**) Autoradiogram of the 12% TBE–PAGE with the 5′- and 3′-overhang substrates. Different AtSRS2 concentrations were used (4, 1, 0.5 and 0.25 nM) and 2 nM AtSRS2-K273R. Reactions were performed using 5.4 mM MgCl$_2$. Samples were incubated for 10 min. (**C**) Illustration of the quantification of the relative concentration of displaced oligonucleotides.

## Minimal length of the 3′-overhang for strand displacement

We further investigated the minimal length of the 3′-overhang that is required to separate the 40-bp duplex region. To this end, we designed seven DNA substrates that differed in the number of nucleotides in the 3′-overhang, and a blunt-end substrate. As in van Komen *et al.* (23), the 3′-overhangs consisted only of thymines and were 2, 5, 8, 10, 12 and 16 nt in length, whereas the 40-nt 3′-overhang was composed of all four bases. The results in Figure 3D illustrate that AtSRS2 needs at least a 16-nt long 3′-tail to separate the 40-bp duplex region, and that an even longer 3′-tail enhances further separation. As expected, no strand displacement was observed with the mutated form of AtSRS2, AtSRS2-K273R, under the chosen conditions.

## AtSRS2 processes nicked HJs

Since former studies of yeast SRS2 reveal a role in DNA repair through SDSA, we designed branched DNA structures that imitate recombinogenic DNA structures that can evolve as intermediates during DNA repair through HR. We tested a variety of HJs that differed in their mobility (partially mobile HJ, static HJ, nicked static HJ) and in the length of the duplex region, and we also designed branched structures according to Dupaigne

*et al.* (24). In order to assign the emerging intermediate structures, we performed gel analyses with the different annealed oligonucleotides and used them as references for the corresponding branched structures on the same gels (Supplementary Data and Supplementary Figure S2). As Figure 4 illustrates, AtSRS2 is able to process several branched DNA structures. Moreover, we found that there were significant differences in disrupting the branched DNA structures. AtSRS2 was able to disrupt the static nicked HJ (X0-nHJ), but we could not detect significant disruption of the static HJ (X0-HJ) without a nick (Figure 4, compare panels A and B). AtSRS2 was also able to disrupt a partially mobile X12-HJ with 12 bp of homology in the center of the HJ (data not shown). But in comparison to the disruption of the X12-HJ, the nicked HJ is a better substrate for AtSRS2. Since the 25-bp duplex regions of each DNA arm of the X12-HJ are shorter when compared with the static X0-HJ (31 bp), one could assume that the better disruption of the X12-HJ is due to the shorter duplex region. Therefore, we tested the disruption of a static nHJ and HJ that consisted of a 24-bp long duplex region. AtSRS2 processed those branched structures in the order X0–nHJ ≫ X12–HJ > X0–HJ and concluded that the better disruption of the X12–HJ compared with the 31-bp long X0–HJ is not due to differences in the duplex lengths.
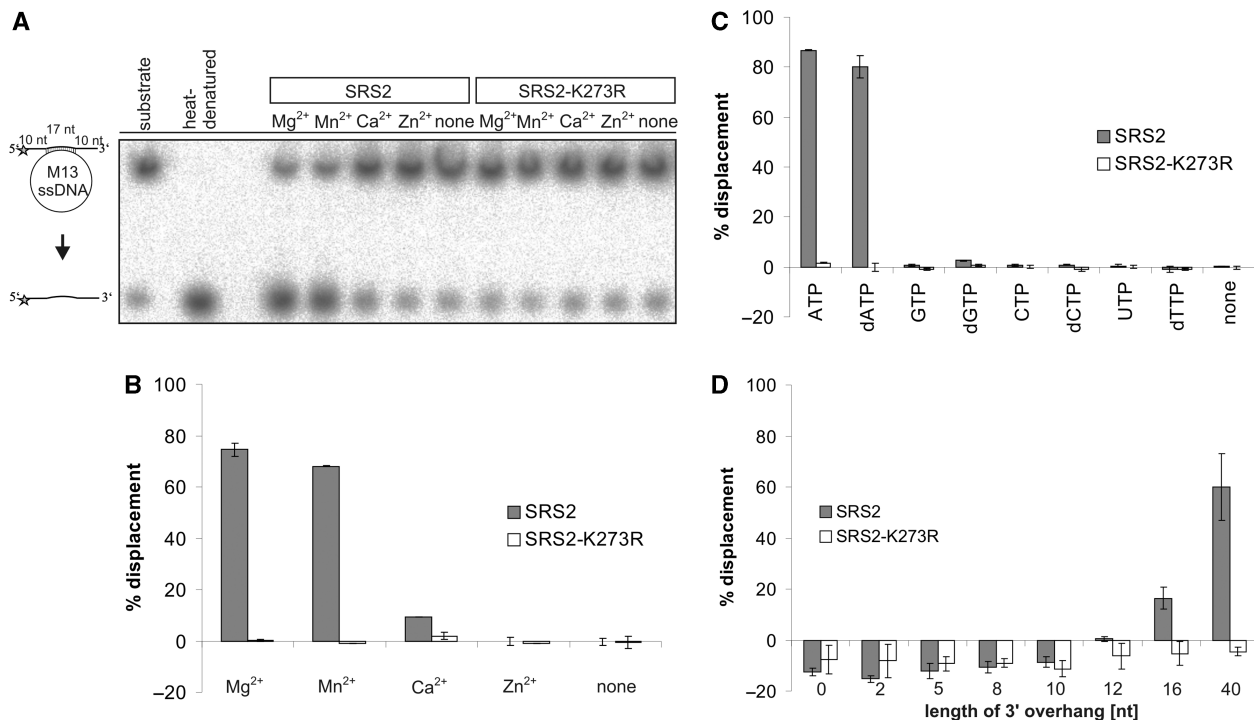
**Figure 3.** Analyses of several basic properties of AtSRS2. (A and B) Illustration of the requirement of different divalent metal cofactors for strand displacement activity of AtSRS2. $MgCl_2$ was substituted by $MnCl_2$, $CaCl_2$ or $ZnCl_2$, (1.8 mM) and alternatively water, and 1.8 mM ATP were used as NTP-cofactors. (**A**) Autoradiogram of the 12% TBE–PAGE. (**B**) Corresponding quantifications. (**C**) Quantification of the (d)NTP requirement for strand displacement of the M13-based substrate. 1.8 mM ATP were substituted by 1.8 mM dATP, GTP, dGTP, CTP, dCTP, UTP, dTTP or water, respectively and 1.8 mM $MgCl_2$ were used as metal-cofactors. Four nM AtSRS2 and 2 nM AtSRS2-K273R were used for analyzing the metal ion and (d)NTP requirement. (**D**) Minimal length of the 3'-overhang for disrupting a 40-bp duplex region in the presence of 11 nM AtSRS2 and 2 nM AtSRS2-K273R, 5.4 mM $MgCl_2$ and 1.8 mM ATP. Each assay was incubated for 10 min. The asterisk indicates the position of the P-32 label.

## AtSRS2 processes PX junctions efficiently

The findings mentioned above led us to the following question: would a PX junction that consists of a single stranded area be an even better substrate for AtSRS2? Therefore, we designed a PX junction according to Dupaigne *et al.* (24). Panel C in Figure 4 illustrates that AtSRS2 disrupts the PX junction far better than the X0–nHJ and X0–HJ. To analyze the way of the disruption, we performed time course experiments of the X0–nHJ, X0–HJ and the PX junction, all consisting of a 31-bp long duplex region. Supplementary Figure S3 shows the time course experiments of AtSRS2 disrupting the PX junction with different labeled oligonucleotides. In the first 5 min of disruption of the PX junction, different products emerge. The first product that emerges is the X0–1 oligonucleotide and the intermediate product consisting of the oligonucleotides X0–2 + 3 + 4a. AtSRS2 processes this intermediate structure in such a way that it displaces the X0–2 oligonucleotide and finally the short X0–4a oligonucleotide. Similar results were obtained with the nicked X0–nHJ (data not shown), except that the emerging X0–1 + 4b intermediate with the 5'-overhang was not processed any further.

## AtSRS2 is able to promote ssDNA pairing

It is thought that during DNA repair by SDSA, the elongated invading strand is displaced by the action of AtSRS2 before it re-anneals to the ssDNA of the other side of the break. We addressed the following question: could AtSRS2 also play a role in the re-annealing of the elongated ssDNA to the ssDNA on the other side of the break? To test if AtSRS2 is able to pair two molecules of ssDNA, we performed strand annealing assays. We tested whether annealing occurred under similar conditions as for strand displacement. To this end, we tested different $MgCl_2$ concentrations for optimal strand pairing and analyzed strand annealing over the course of time. We found that annealing of a 40-nt oligonucleotide with a 80-nt oligonucleotide occurs over a broad range of $MgCl_2$ concentrations in the reaction buffer. We also found that maximal annealing is obtained after 20 min at 30°C (data not shown). Therefore, we carried out further experiments under similar conditions to those used for the helicase assays, using 5.4 mM $MgCl_2$ in the reaction buffer.

To verify that it is hybridization that is being measured and not protein binding, we performed control experiments. Supplementary Figure S4 shows that the products of the SRS2-dependent annealing reaction run on the same level as the annealed oligonucleotides on the gel. Additionally, we carried out reactions without the non-labeled complementary oligonucleotide, and we did not detect any band-shift after the gelelectrophoresis (Supplementary Figure S4, lanes C1 and C2). Figure 5
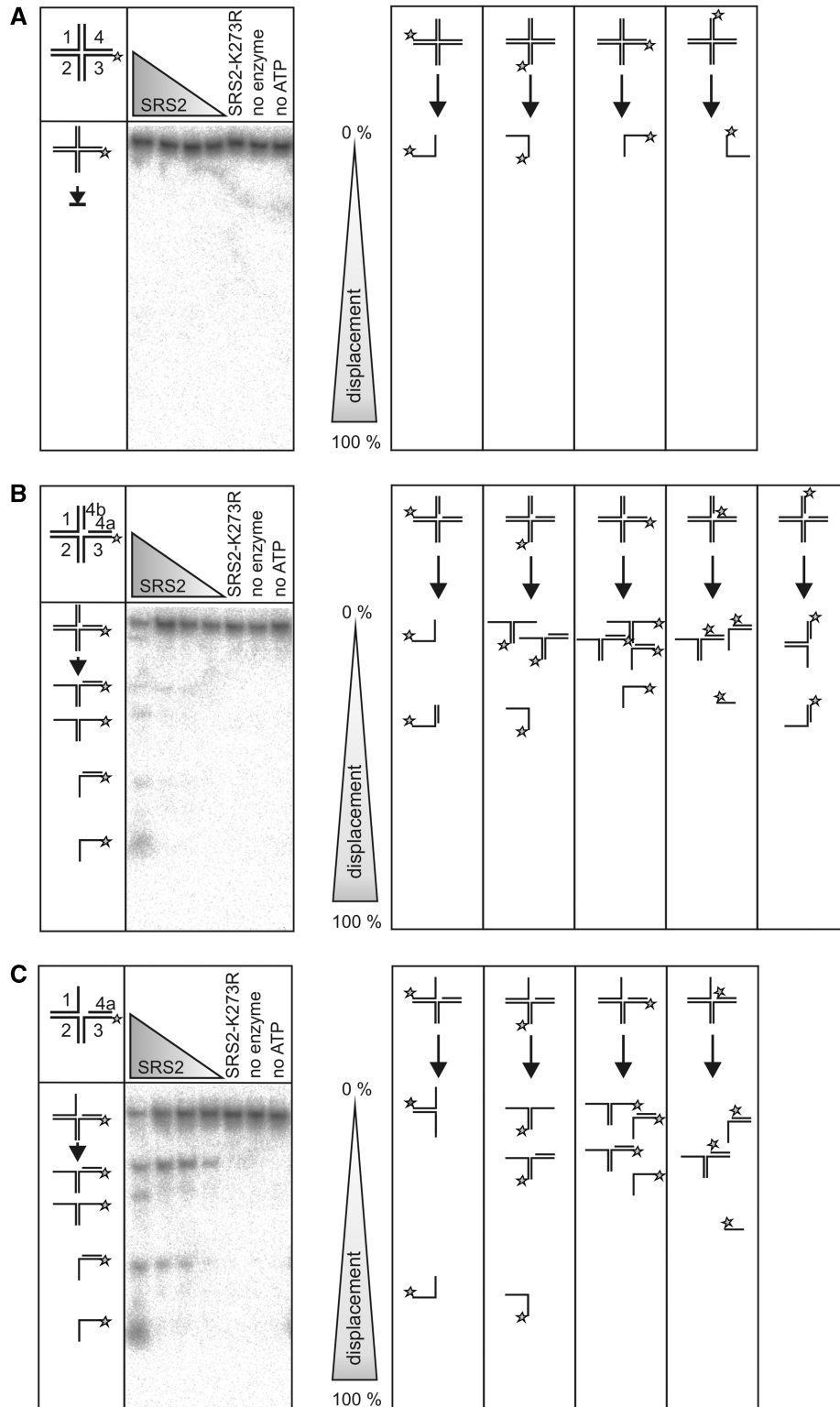
**Figure 4.** AtSRS2 disrupts branched DNA structures. (**A**) X0–HJ, (**B**) X0–nHJ, (**C**) PX-junction. Helicase assays were performed with 8, 3, 2 and 1.5 nM AtSRS2, 2 nM AtSRS2-K273R, 1.8 mM MgCl₂ and 1.8 mM ATP and incubated at 30°C for 20 min. The samples without ATP in the reaction were carried out with 8 nM AtSRS2. On the left side of Panels A, B and C are examples of autoradiograms of each junction with an X0-3* labeled oligonucleotide. The right side illustrates schematically the experimentally findings of all products that evolve during disruption of the different junctions. The triangle displays the percentage of displacement of the resulting products (from 0% displacement to 100% displacement). The asterisk indicates the position of the P-32 label.
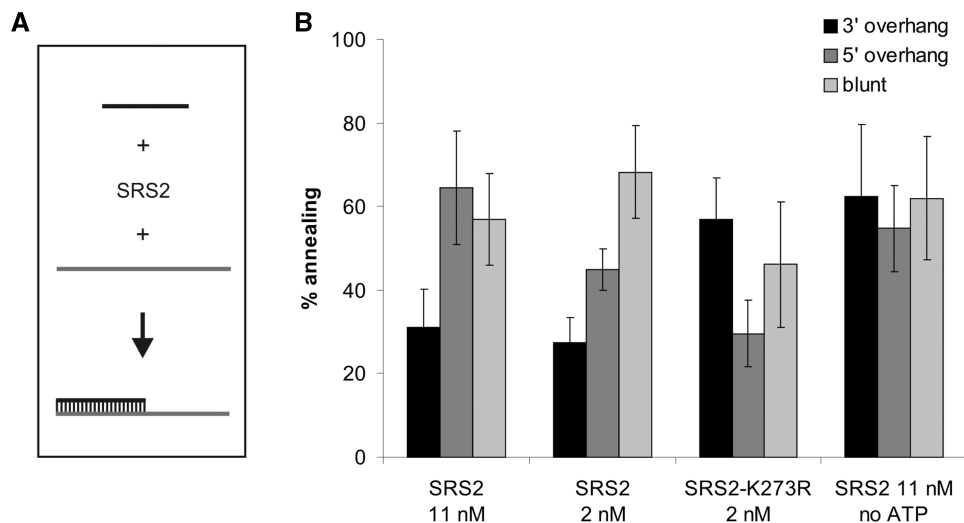
**Figure 5.** AtSRS2-dependent single strand annealing. (**A**) Scheme of the annealing reaction. (**B**) Quantification of strand pairing by AtSRS2. Reactions were carried out as described in 'Materials and Methods' section.
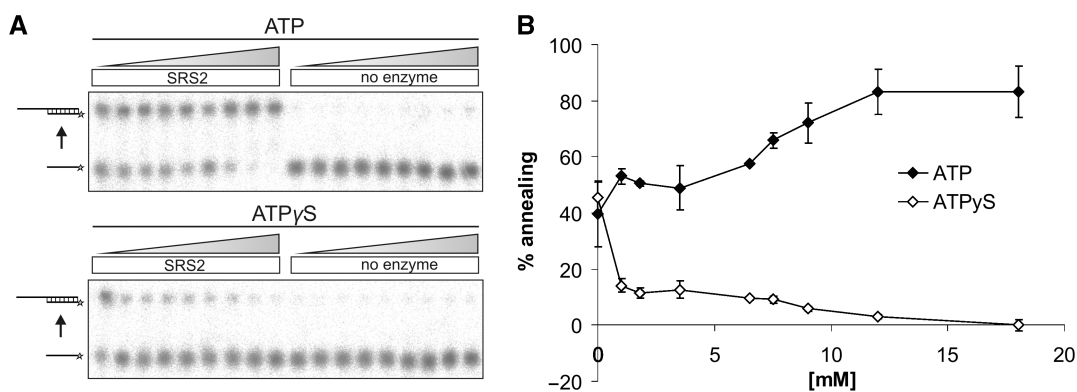


**Figure 6.** Influence of ATP and ATPγS on the annealing reaction. (**A**) Concentration-dependent annealing reaction with 0, 1, 1.8, 3.5, 6.5, 7.5, 9, 12 and 18 mM ATP or ATPγS in the reaction, 8 nM AtSRS2 and respectively, no enzyme. The emerging DNA product is a 5'-overhang substrate with 40-nt overhang and a 40-bp duplex region. (**B**) Quantification of ATP and ATPγS-dependent annealing reactions. The assays ran under the conditions as described in 'Materials and Methods' section.

illustrates that ssDNA annealing occurs with oligo-nucleotides that result in a blunt-end, 3'- or 5'-overhang DNA substrate with a 40-bp duplex region. The graph also demonstrates that the AtSRS2-dependent annealing of the 3'-overhang oligonucleotide is reduced compared with the annealing reactions with the oligonucleotides that result in blunt-end or 5'-overhang substrates, but is increased by AtSRS2-K273R and without ATP in the reaction buffer. Moreover, it is noticeable that ssDNA annealing occurs with all analyzed oligonucleotides even without ATP in the reaction buffer, and AtSRS2-K273R is also able to promote ssDNA annealing.

### Influence of NTPs on the annealing reaction

Since AtSRS2 requires ATP hydrolysis to separate dsDNA, and strand pairing occurs without ATP in the reaction buffer, we addressed the question of whether strand annealing is influenced by other NTP co-substrates. Therefore, we performed concentration-dependent strand pairing assays with ATP, ATPγS, ADP and AMP. In order to prevent antagonistic strand displacement activity, we used oligonucleotides whose products resulted in a 40-bp duplex region with a 40-nt 5'-overhang. We observed a constant increase in AtSRS2-dependent strand annealing with increased ATP concentrations of up to 18 mM in the reaction buffer. If we used the poorly hydrolyzable ATP analog ATPγS in the reaction, strand annealing strongly decreased with increasing concentrations of ATPγS until no annealing was observed at 18 mM ATPγS (Figure 6). Concentrations of up to 18 mM ADP and AMP in the reaction showed a slightly increase in strand annealing with increasing ADP concentration and a slight inhibition of strand annealing with increasing AMP concentration (data not shown).
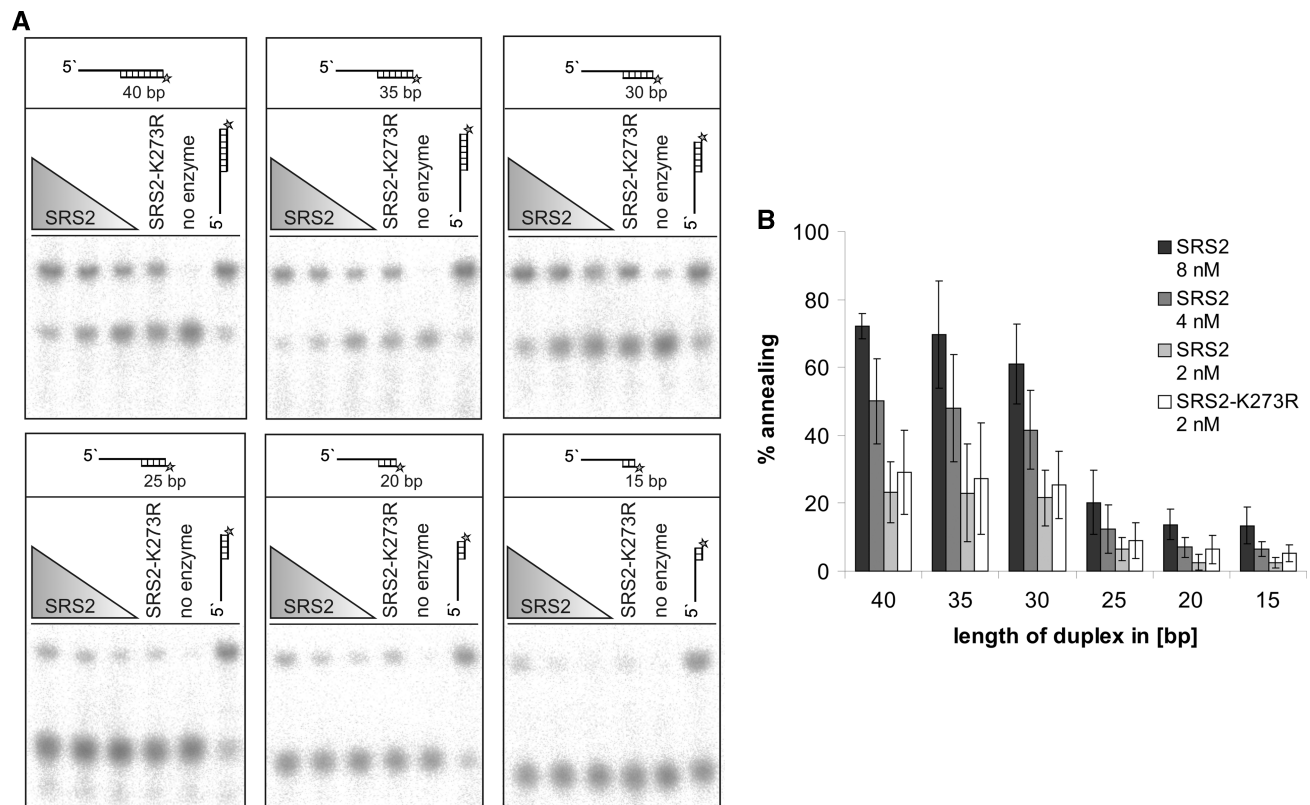
**Figure 7.** Strand pairing is influenced by the length of the emerging duplex region. (**A** and **B**) Reactions were performed with different oligonucleotides resulting in different DNA products after single strand annealing. The oligonucleotides were designed so that the resulting products differed in their length in the duplex region, but not in the length of the 5′-overhang (40 nt).

### Strand annealing by AtSRS2 is dependent on the duplex length

We next studied the influence of the length of the emerging duplex region on the efficiency of AtSRS2-mediated strand annealing. The emerging DNA substrates consisted of 40-nt 5′-overhangs and differed in the length of the duplex region. We found that little strand pairing took place at a duplex length of 20 and 15 bp. Increasing oligonucleotide length in the complementary region revealed an increase in strand pairing by AtSRS2 (Figure 7A and B). We did not detect further enhancement of the annealing activity by enlarging the duplex region up to 35 and 40 bp. Calculating the corresponding melting temperatures of the emerging duplex regions according to the Nearest-Neighbor model demonstrated that all duplexes should be stable at the incubation temperature (see Supplementary Data, Table S1).

### DISCUSSION

Former studies of SRS2 in yeast revealed a significant role in DNA repair through HR. Homologs of SRS2 are the bacterial helicases UVRD, REP and PCRA (6,7). Genetic and biochemical studies indicate that SRS2 can act as an antirecombinase (17–21,24). Aside from this function, SRS2 is supposed to function as an activator of the postreplicative DNA repair pathway, and it also plays a role in DNA damage checkpoint-mediated cell cycle arrest (10–12,38,39). Most studies of SRS2 have been done in yeast, but thus far, there are no data available for SRS2 from a multicellular eukaryote. In this study, we analyzed the enzymatic behavior of the plant SRS2 homolog from *A. thaliana*.

For our biochemical characterization, we purified the recombinant AtSRS2 and a mutant form of AtSRS2, AtSRS2-K273R. AtSRS2-K273R features a substitution of lysine to arginine in the Walker A motif. Mutations in the Walker A motif result in loss of the ATPase- and helicase activity of DNA helicases (34,40) and hence AtSRS2-K273R can serve as a negative control. We observed displacement activity with the purified AtSRS2 2protein, but we did not detect displacement without AtSRS2 or ATP in the reaction (Figure 2A). Additionally, no disruption occurred with the recombinant AtSRS2-K273R. The results demonstrate that the purified AtSRS2 is a functional helicase and that AtSRS2-K273R can be used as a negative control for further studies.

Next, we defined the reaction conditions in which optimal strand displacement occurred. Interestingly, we observed almost no difference in the strand displacement activity of AtSRS2 at different incubation temperatures, and even observed helicase activity at 4°C (data not shown). Therefore, we designate AtSRS2 as a temperature-tolerant helicase.

To begin the study of the basic properties of AtSRS2, we first analyzed the direction in which the helicase processes DNA substrates. Similar to most helicases, AtSRS2 features a specific directionality, and that is a 3′- to 5′-direction (Figure 2B and C). The REP helicase from *E. coli* can also be classified as a 3′- to 5′-helicase (41) as can ScSRS2 (22). It seems that AtSRS2 is a 3′- to 5′-helicase in a stricter sense than SRS2 from *S. cerevisiae*. Van Komen *et al.* (23) were able to show that ScSRS2 is also able to act on substrates with 5′-overhangs or on blunt-end substrates but prefers to unwind substrates with 3′-overhangs. They therefore classified ScSRS2 as a 3′- to 5′-helicase, as was already shown by Rong and Klein (22). The SRS2 homologs, UVRD and PCRA, also demonstrate unwinding of 5′-overhang substrates whereas UVRD preferentially unwinds 3′-overhang substrates (42,43). PCRA can act in both directions (44–46). To test whether AtSRS2 is also able to act on 5′-overhang and blunt-end DNA substrates, we modified the reaction conditions, but AtSRS2 processed only the 3′-overhang substrates and therefore has to be classified as a 3′- to 5′-helicase.

Next, we investigated the dependence of the helicase reaction of AtSRS2 on divalent metal cations. Like most helicases, the strand displacement activity of AtSRS2 is dependent on the presence of $Mg^{2+}$ which can be substituted by $Mn^{2+}$ whereas little unwinding occurred with $Ca^{2+}$, and no unwinding with $Zn^{2+}$ (Figure 3A and B). Similar results were obtained with ScSRS2 (22,23), whereas MtUVRD from *Mycobacterium tuberculosis* did not show DNA unwinding in the presence of $Ca^{2+}$ (43).

Helicases have also been shown to prefer specific nucleotide co-substrates for their helicase activity. Therefore, we measured the strand displacement activity of AtSRS2 with different NTPs and dNTPs. Consistent with the SRS2 homolog ScSRS2 (22,23) and UVRD from *E. coli* and *M. tuberculosis* (43,47), we did observe strand displacement with ATP and dATP, whereas the other (d)NTPs did not support strand unwinding. In contrast, the replicative helicase REP also showed strand displacement with GTP, dGTP, and to a lesser extent with CTP, dCTP, UTP and dTTP, but preferred ATP and dATP for the helicase reaction (48). The helicase PCRA from *B. stearothermophilus* was also able to hydrolyze a wide range of nucleotides (49).

Moreover, we defined the minimal length of a 3′-overhang that is necessary for unwinding of a 40-bp duplex region. We found that AtSRS2 needs at least a 16-nt long 3′-overhang for productive unwinding of a 40-bp duplex region (Figure 3D). This is in contrast to ScSRS2, which promotes DNA unwinding with even a 2-nt 3′-overhang with the same DNA substrates tested (23). UVRD from *M. tuberculosis* disrupts DNA substrates consisting of a 12-bp duplex region if the 3′-overhangs are at least 12 nt long (43) and the bipolar PCRA helicase from *S. aureus* is able to promote unwinding of a DNA substrate that consisted of 4-nt long 5′-overhangs on both ends (44).

Since genetic and biochemical data indicate a role for SRS2 in suppressing crossovers during double-strand break repair (17,24,50), we addressed whether the plant

AtSRS2 helicase features a similar function. To this end, we designed different branched structures (X0–HJ, X0–nHJ, X12–HJ and PX junction) that can evolve during the repair of DSBs by HR (24,35–37,51). The analyzed X0–nHJ is an intermediate structure that can evolve during the repair of DSBs according to the classical DSBR model (4,52,53). The PX junction resembles the intermediate structure that is formed during DNA repair according to the SDSA model (24,53–56). Intact HJs also play a central role in HR. In synthetic partially mobile HJs, e.g. the X12–HJ, the branch point can move. Therefore, those structures are often used to study branch migration (57,58).

As we tested the helicase activity on the branched DNA substrates, we found that AtSRS2 was actually able to disrupt most branched structures (Figure 4). Moreover, we were able to show that AtSRS2 prefers to unwind the PX junction compared with the X0–nHJ (Figure 4) and X12–HJ (data not shown), whereas little to no unwinding was detected with the X0–HJ (Figure 4). Similar results were obtained with ScSRS2 (24), but no further data that describe the disruption of HJs or PX junctions by SRS2 homologs are available. Since we observed that a nick or an homologous central region increases the disruption of the branched structures by AtSRS2, and that a PX junction containing a single stranded area is an even better substrate for AtSRS2, we concluded that a nick or temporary gap caused by movement of the homologous area in the center of the X12–HJ yields small openings for AtSRS2 to bind and displace the oligonucleotides of the branched substrates. Inspired by these observations, we performed time course experiments with those substrates containing differently labeled oligonucleotides in order to follow the appearance of the different products, thus getting an indication of the way of HJ disruption by AtSRS2. As shown in the Supplementary Figure S3, we observed that disruption of the PX junction resulted in different products that increased or decreased over the course of time. The order and the amount of products that emerged led us to the model shown in Figure 8. First, AtSRS2 binds the accessible ssDNA providing a 3′-tail (A), which is in accordance with the directionality of AtSRS2. After displacement of the first oligonucleotide, an intermediate structure emerges that is captured by AtSRS2, followed by displacement of the next oligonucleotide in the 3′- to 5′-direction (B). Finally, AtSRS2 disrupts the last intermediate structure starting from the 3′-end (C). We observed similar results with the X0–nHJ (data not shown), except that the first product was not ssDNA, but a partial duplex intermediate with a 5′-overhang. We concluded that AtSRS2 could not disrupt this intermediate due to its directionality. The way by which AtSRS2 disrupts the PX junction and to a lesser extent the X0–nHJ/X12–HJ supports the assumption that the plant SRS2 homolog, AtSRS2, functions in HR. Moreover, our detailed analyses of the PX junction disassembly by the plant helicase AtSRS2 clearly support the model put forth by Dupaigne *et al.* (24).

Additionally, we were able to demonstrate that disruption of the HJ is not due to branch migration, as the
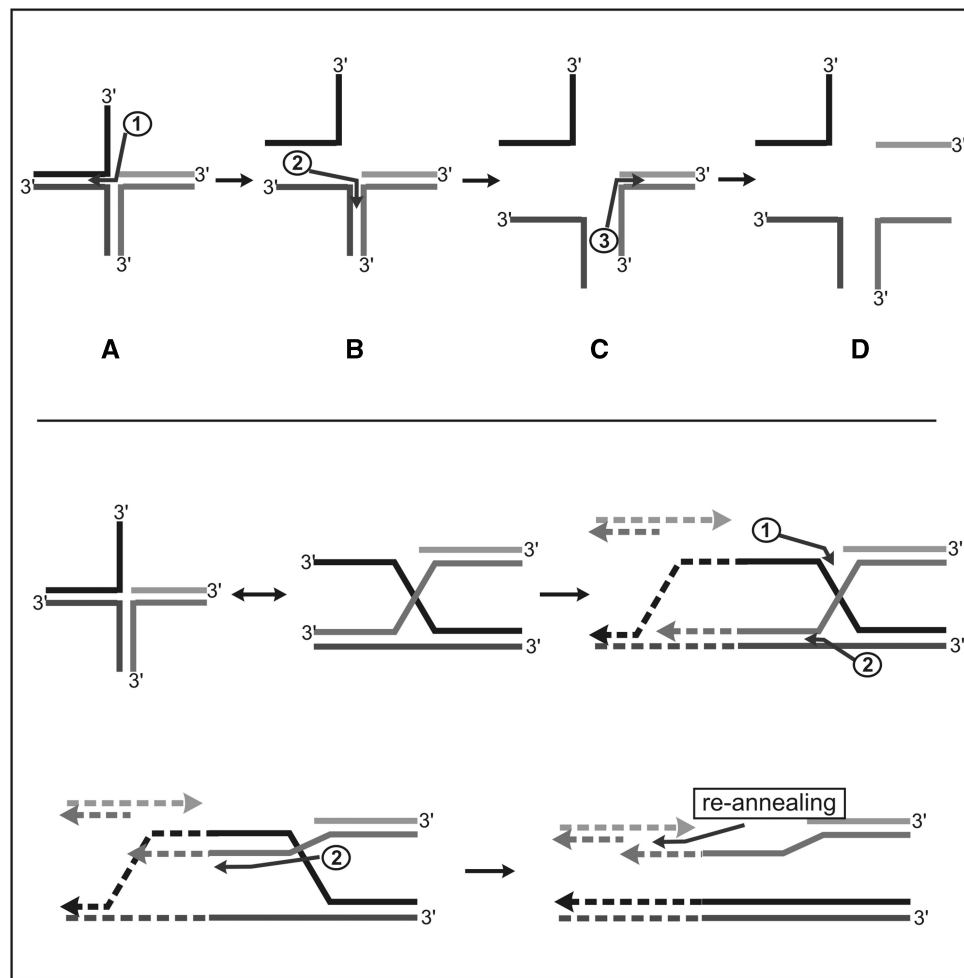
**Figure 8.** Disruption of the PX junction. (**A**) AtSRS2 displaces the accessible ssDNA in 3′- to 5′-direction and works its way through the junction, while disrupting the emerging 3′-overhang intermediates (**B–D**). The first two steps of the PX junction disruption can be translated into the displacement of the invaded ssDNA by the SDSA model (lower part). Furthermore, AtSRS2 could play a role in the re-annealing of the displaced, elongated ssDNA.

resulting product of the X12–HJ disruption is ssDNA and not splayed arm (data not shown). In contrast to SRS2, most RECQ helicases produce a splayed arm as the main product of HJ disruption, assuming the processing of HJs through branch migration (32,58–60).

Furthermore, we addressed the question of whether the AtSRS2 helicase is able to perform re-annealing. To date, no SRS2-dependent annealing has been demonstrated, but many studies of helicase-dependent annealing were done with RECQ helicases (58,59,61–63). Moreover, Machwe et al. have shown that strand pairing is not present in all helicases, since the SRS2 homolog EcUVRD and the viral NS3 enzyme did not promote ssDNA annealing (64). We were able to show that AtSRS2-dependent annealing occurred with overhang and blunt-end substrates (Figure 5B), and furthermore verified that we measured hybridization and not protein-binding causing a band-shift on the gel (Supplementary data and Supplementary Figure S4). Hybridization does not occur in the absence of AtSRS2 or AtSRS2-K273R probably due to low oligonucleotide concentration, since we

observed a slightly increase of spontaneous hybridization with increasing oligonucleotide concentrations (data not shown). Noticeably less annealing occurred with oligonucleotides that led to a 3′-overhang substrate (Figure 5B). We, therefore, concluded that this decreased single strand annealing is due to the antagonistic activities of the helicase and annealing reactions, since AtSRS2 is unable to disrupt substrates with a blunt-end or 5′-end. Moreover, the annealing of ssDNA resulting in 3′-overhang substrates increased without ATP in the reaction or with AtSRS2-K273R. The assumption that AtSRS2 combines its helicase activity with its ability to anneal ssDNA in a concerted action has also been predicted for the RECQ helicases HsWRN, HsBLM and DmRECQ5β, where this feature could be applied in the processing of a HJ through branch migration and for replication fork regression (64). The observation that AtSRS2 can promote ssDNA pairing without ATP or with AtSRS2-K273R demonstrates that the proteins are still able to interact with DNA. This assumption is supported by Krejci *et al.* (34), who have shown that a mutated form

of ScSRS2, consisting of a substitution in the Walker A motif, retained DNA binding, and also that DNA binding by SRS2 and the mutated srs2 proteins was not influenced by ATP.

Since the ATPase-deficient helicase AtSRS2-K273R also facilitates strand annealing, we assume that this reaction is independent of the hydrolysis of ATP but could depend on conformational changes of both proteins caused by the different binding status of NTPs.

We therefore studied the influence of ATP, ATPγS, ADP and AMP on the annealing reaction (Figure 6). Our observations that increasing amounts of ATP increased and ATPγS decreased the strand pairing reaction support our hypothesis mentioned above. The poorly hydrolyzable ATP analog ATPγS keeps the protein in the ATP-bound mode, probably leading to a conformation that impairs or prevents ssDNA pairing. However, after the hydrolysis of ATP, the binding mode changes, which is followed by a conformational change of the helicase promoting ssDNA pairing. The observations that ADP also promotes the annealing reaction and AMP inhibits the reaction support our assumption. Moreover, Sharma *et al.* (58) have shown with hRECQ1 that ATP binding leads to a conformational change and suggested that a nucleotide-induced conformational change could be a trigger to switch from helicase to annealing activity. Hence, we conclude that a conformational change due to NTP binding could have a significant effect on AtSRS2-dependent ssDNA pairing.

Next we investigated whether the length of the duplex region influences the ssDNA pairing reaction. The melting temperatures of the emerging duplex regions of the different products were all above the incubation temperature (Table S1), and therefore decreasing annealing was not due to denaturation of the products. We observed that ssDNA pairing increased with increasing duplex length (Figure 7). Similar results were obtained with the helicase HsBLM, where little annealing was observed with oligonucleotides that yielded a duplex length of 15 bp, and maximal annealing was observed with a duplex length of 50 bp. In accordance with Cheok *et al.* (61), we assume that the influence of the oligonucleotide length could be due to the stable binding of AtSRS2 on ssDNA.

In summary, we identified an AtSRS2 homolog in the plant model organism *A. thaliana*, and our biochemical studies reveal a function in the disruption of recombination intermediates and in strand annealing. It is tempting to speculate that AtSRS2 might play a role in the re-annealing of displaced ssDNA by the SDSA pathway (Figure 8). Therefore, it will be interesting to define the role of AtSRS2 *in planta* and to test whether the protein is involved in SDSA-like or other recombination reactions *in vivo*.

## ACCESSION NUMBER

GQ148553.

## SUPPLEMENTARY DATA

Supplementary Data are available at NAR Online.

## REFERENCES

1. Caruthers,J.M. and McKay,D.B. (2002) Helicase structure and mechanism. *Curr. Opin. Struct. Biol.*, **12**, 123–133.
2. Tuteja,N. and Tuteja,R. (2004) Unraveling DNA helicases. Motif, structure, mechanism and function. *Eur. J. Biochem.*, **271**, 1849–1863.
3. Wu,L. and Hickson,I.D. (2006) DNA helicases required for homologous recombination and repair of damaged replication forks. *Annu. Rev. Genet.*, **40**, 279–306.
4. Puchta,H. (2005) The repair of double-strand breaks in plants: mechanisms and consequences for genome evolution. *J. Exp. Bot.*, **56**, 1–14.
5. Hartung,F. and Puchta,H. (2006) The RecQ gene family in plants. *J. Plant Physiol.*, **163**, 287–296.
6. Aboussekhra,A., Chanet,R., Zgaga,Z., Cassier-Chauvat,C., Heude,M. and Fabre,F. (1989) RADH, a gene of *Saccharomyces cerevisiae* encoding a putative DNA helicase involved in DNA repair. Characteristics of radH mutants and sequence of the gene. *Nucleic Acids Res.*, **17**, 7211–7219.
7. Shankar,J. and Tuteja,R. (2008) UvrD helicase of *Plasmodium falciparum*. *Gene*, **410**, 223–233.
8. Lawrence,C.W. and Christensen,R.B. (1979) Metabolic suppressors of trimethoprim and ultraviolet light sensitivities of *Saccharomyces cerevisiae* rad6 mutants. *J. Bacteriol.*, **139**, 866–876.
9. Aguilera,A. and Klein,H.L. (1988) Genetic control of intrachromosomal recombination in *Saccharomyces* cerevisiae. I. Isolation and genetic characterization of hyper-recombination mutations. *Genetics*, **119**, 779–790.
10. Papouli,E., Chen,S., Davies,A.A., Huttner,D., Krejci,L., Sung,P. and Ulrich,H.D. (2005) Crosstalk between SUMO and ubiquitin on PCNA is mediated by recruitment of the helicase Srs2p. *Mol. Cell*, **19**, 123–133.
11. Pfander,B., Moldovan,G.L., Sacher,M., Hoege,C. and Jentsch,S. (2005) SUMO-modified PCNA recruits Srs2 to prevent recombination during *S* phase. *Nature*, **436**, 428–433.
12. Schiestl,R.H., Prakash,S. and Prakash,L. (1990) The SRS2 suppressor of rad6 mutations of *Saccharomyces cerevisiae* acts by channeling DNA lesions into the RAD52 DNA repair pathway. *Genetics*, **124**, 817–831.
13. Rong,L., Palladino,F., Aguilera,A. and Klein,H.L. (1991) The hyper-gene conversion hpr5-1 mutation of *Saccharomyces cerevisiae* is an allele of the SRS2/RADH gene. *Genetics*, **127**, 75–85.
14. Aboussekhra,A., Chanet,R., Adjiri,A. and Fabre,F. (1992) Semidominant suppressors of Srs2 helicase mutations of *Saccharomyces cerevisiae* map in the RAD51 gene, whose sequence

predicts a protein with similarities to procaryotic RecA proteins.*Mol. Cell Biol.*, **12**, 3224–3234.

15. Milne,G.T., Ho,T. and Weaver,D.T. (1995) Modulation of *Saccharomyces cerevisiae* DNA double-strand break repair by SRS2 and RAD51. *Genetics*, **139**, 1189–1199.

16. Chanet,R., Heude,M., Adjiri,A., Maloisel,L. and Fabre,F. (1996) Semidominant mutations in the yeast Rad51 protein and their relationships with the Srs2 helicase. *Mol. Cell Biol.*, **16**, 4782–4789.

17. Ira,G., Malkova,A., Liberi,G., Foiani,M. and Haber,J.E. (2003) Srs2 and Sgs1-Top3 suppress crossovers during double-strand break repair in yeast. *Cell*, **115**, 401–411.

18. Ira,G. and Haber,J.E. (2002) Characterization of RAD51-independent break-induced replication that acts preferentially with short homologous sequences. *Mol. Cell Biol.*, **22**, 6384–6392.

19. Aylon,Y., Liefshitz,B., Bitan-Banin,G. and Kupiec,M. (2003) Molecular dissection of mitotic recombination in the yeast *Saccharomyces cerevisiae*. *Mol. Cell Biol.*, **23**, 1403–1417.

20. Veaute,X., Jeusset,J., Soustelle,C., Kowalczykowski,S.C., Le Cam,E. and Fabre,F. (2003) The Srs2 helicase prevents recombination by disrupting Rad51 nucleoprotein filaments. *Nature*, **423**, 309–312.

21. Krejci,L., Van Komen,S., Li,Y., Villemain,J., Reddy,M.S., Klein,H., Ellenberger,T. and Sung,P. (2003) DNA helicase Srs2 disrupts the Rad51 presynaptic filament. *Nature*, **423**, 305–309.

22. Rong,L. and Klein,H.L. (1993) Purification and characterization of the SRS2 DNA helicase of the yeast *Saccharomyces cerevisiae*. *J. Biol. Chem.*, **268**, 1252–1259.

23. Van Komen,S., Reddy,M.S., Krejci,L., Klein,H. and Sung,P. (2003) ATPase and DNA helicase activities of the *Saccharomyces cerevisiae* anti-recombinase Srs2. *J. Biol. Chem.*, **278**, 44331–44337.

24. Dupaigne,P., Le Breton,C., Fabre,F., Gangloff,S., Le Cam,E. and Veaute,X. (2008) The Srs2 helicase activity is stimulated by Rad51 filaments on dsDNA: implications for crossover incidence during mitotic recombination. *Mol. Cell*, **29**, 243–254.

25. Wang,S.W., Goodwin,A., Hickson,I.D. and Norbury,C.J. (2001) Involvement of *Schizosaccharomyces pombe* Srs2 in cellular responses to DNA damage. *Nucleic Acids Res.*, **29**, 2963–2972.

26. Doe,C.L. and Whitby,M.C. (2004) The involvement of Srs2 in post-replication repair and homologous recombination in fission yeast. *Nucleic Acids Res.*, **32**, 1480–1491.

27. Yasuhira,S. (2009) Redundant roles of Srs2 helicase and replication checkpoint in survival and rDNA maintenance in *Schizosaccharomyces pombe*. *Mol. Genet. Genomics*, **281**, 497–509.

28. Suzuki,K., Kato,A., Sakuraba,Y. and Inoue,H. (2005) Srs2 and RecQ homologs cooperate in mei-3-mediated homologous recombination repair of *Neurospora crassa*. *Nucleic Acids Res.*, **33**, 1848–1858.

29. Chiolo,I., Saponaro,M., Baryshnikova,A., Kim,J.H., Seo,Y.S. and Liberi,G. (2007) The human F-Box DNA helicase FBH1 faces *Saccharomyces cerevisiae* Srs2 and postreplication repair pathway roles. *Mol. Cell Biol.*, **27**, 7439–7450.

30. Osman,F., Dixon,J., Barr,A.R. and Whitby,M.C. (2005) The F-Box DNA helicase Fbh1 prevents Rhp51-dependent recombination without mediator proteins. *Mol. Cell Biol.*, **25**, 8084–8096.

31. Matz,M., Shagin,D., Bogdanova,E., Britanova,O., Lukyanov,S., Diatchenko,L. and Chenchik,A. (1999) Amplification of cDNA ends based on template-switching effect and step-out PCR. *Nucleic Acids Res.*, **27**, 1558–1560.

32. Kobbe,D., Blanck,S., Demand,K., Focke,M. and Puchta,H. (2008) AtRECQ2, a RecQ helicase homologue from *Arabidopsis thaliana*, is able to disrupt various recombinogenic DNA structures in vitro. *Plant J.*, **55**, 397–405.

33. Kobbe,D., Focke,M. and Puchta,H. (2009) Purification and characterization of RecQ helicases of plants. *Methods Mol. Biol.*, **587**, 195–209.

34. Krejci,L., Macris,M., Li,Y., Van Komen,S., Villemain,J., Ellenberger,T., Klein,H. and Sung,P. (2004) Role of ATP hydrolysis in the antirecombinase function of *Saccharomyces cerevisiae* Srs2 protein. *J. Biol. Chem.*, **279**, 23193–23199.

35. Mohaghegh,P., Karow,J.K., Brosh,R.M. Jr, Bohr,V.A. Jr. and Hickson,I.D. (2001) The Bloom's and Werner's syndrome proteins are DNA structure-specific helicases. *Nucleic Acids Res.*, **29**, 2843–2849.

36. Gaillard,P.H., Noguchi,E., Shanahan,P. and Russell,P. (2003) The endogenous Mus81-Eme1 complex resolves Holliday junctions by a nick and counternick mechanism. *Mol. Cell*, **12**, 747–759.

37. Boddy,M.N., Gaillard,P.H., McDonald,W.H., Shanahan,P., Yates,J.R. III and Russell,P. (2001) Mus81-Eme1 are essential components of a Holliday junction resolvase. *Cell*, **107**, 537–548.

38. Klein,H.L. (2001) Mutations in recombinational repair and in checkpoint control genes suppress the lethal combination of srs2Delta with other DNA repair genes in *Saccharomyces cerevisiae*. *Genetics*, **157**, 557–565.

39. Liberi,G., Chiolo,I., Pellicioli,A., Lopes,M., Plevani,P., Muzi-Falconi,M. and Foiani,M. (2000) Srs2 DNA helicase is involved in checkpoint response and its regulation requires a functional Mec1-dependent pathway and Cdk1 activity. *EMBO J.*, **19**, 5027–5038.

40. Brosh,R.M. Jr, Orren,D.K., Nehlin,J.O., Ravn,P.H., Kenny,M.K., Machwe,A. and Bohr,V.A. (1999) Functional and physical interaction between WRN helicase and human replication protein A. *J. Biol. Chem.*, **274**, 18341–18350.

41. Yarranton,G.T. and Gefter,M.L. (1979) Enzyme-catalyzed DNA unwinding: studies on *Escherichia coli* rep protein. *Proc. Natl Acad. Sci. USA*, **76**, 1658–1662.

42. An,L., Tang,W., Ranalli,T.A., Kim,H.J., Wytiaz,J. and Kong,H. (2005) Characterization of a thermostable UvrD helicase and its participation in helicase-dependent amplification. *J. Biol. Chem.*, **280**, 28952–28958.

43. Curti,E., Smerdon,S.J. and Davis,E.O. (2007) Characterization of the helicase activity and substrate specificity of *Mycobacterium tuberculosis* UvrD. *J. Bacteriol.*, **189**, 1542–1555.

44. Chang,T.L., Naqvi,A., Anand,S.P., Kramer,M.G., Munshi,R. and Khan,S.A. (2002) Biochemical characterization of the *Staphylococcus aureus* PcrA helicase and its role in plasmid rolling circle replication. *J. Biol. Chem.*, **277**, 45880–45886.

45. Naqvi,A., Tinsley,E. and Khan,S.A. (2003) Purification and characterization of the PcrA helicase of Bacillus anthracis. *J. Bacteriol.*, **185**, 6633–6639.

46. Ruiz-Maso,J.A., Anand,S.P., Espinosa,M., Khan,S.A. and del Solar,G. (2006) Genetic and biochemical characterization of the Streptococcus pneumoniae PcrA helicase and its role in plasmid rolling circle replication. *J. Bacteriol.*, **188**, 7416–7425.

47. Matson,S.W. and George,J.W. (1987) DNA helicase II of *Escherichia coli*. Characterization of the single-stranded DNA-dependent NTPase and helicase activities. *J. Biol. Chem.*, **262**, 2066–2076.

48. Kornberg,A., Scott,J.F. and Bertsch,L.L. (1978) ATP utilization by rep protein in the catalytic separation of DNA strands at a replicating fork. *J. Biol. Chem.*, **253**, 3298–3304.

49. Bird,L.E., Brannigan,J.A., Subramanya,H.S. and Wigley,D.B. (1998) Characterisation of *Bacillus stearothermophilus* PcrA helicase: evidence against an active rolling mechanism. *Nucleic Acids Res.*, **26**, 2686–2693.

50. Robert,T., Dervins,D., Fabre,F. and Gangloff,S. (2006) Mrc1 and Srs2 are major actors in the regulation of spontaneous crossover. *EMBO J.*, **25**, 2837–2846.

51. Geuting,V., Kobbe,D., Hartung,F., Durr,J., Focke,M. and Puchta,H. (2009) Two distinct MUS81–EME1 complexes from Arabidopsis process Holliday junctions. *Plant Physiol.*, **150**, 1062–1071.

52. Szostak,J.W., Orr-Weaver,T.L., Rothstein,R.J. and Stahl,F.W. (1983) The double-strand-break repair model for recombination. *Cell*, **33**, 25–35.

53. Paques,F. and Haber,J.E. (1999) Multiple pathways of recombination induced by double-strand breaks in *Saccharomyces cerevisiae*. *Microbiol. Mol. Biol. Rev.*, **63**, 349–404.

54. Puchta,H. (1999) Double-strand break-induced recombination between ectopic homologous sequences in somatic plant cells. *Genetics*, **152**, 1173–1181.

55. Formosa,T. and Alberts,B.M. (1986) DNA synthesis dependent on genetic recombination: characterization of a reaction catalyzed by purified bacteriophage T4 proteins. *Cell*, **47**, 793–806.

56. Nassif,N., Penney,J., Pal,S., Engels,W.R. and Gloor,G.B. (1994) Efficient copying of nonhomologous sequences from ectopic sites via P-element-induced gap repair. *Mol. Cell Biol.*, **14**, 1613–1625.

57. Parsons,C.A., Tsaneva,I., Lloyd,R.G. and West,S.C. (1992) Interaction of *Escherichia coli* RuvA and RuvB proteins with synthetic Holliday junctions. *Proc. Natl Acad Sci. USA*, **89**, 5452–5456.

58. Sharma,S., Sommers,J.A., Choudhary,S., Faulkner,J.K., Cui,S., Andreoli,L., Muzzolini,L., Vindigni,A. and Brosh,R.M. Jr. (2005) Biochemical analysis of the DNA unwinding and strand annealing activities catalyzed by human RECQ1. *J. Biol. Chem.*, **280**, 28072–28084.

59. Garcia,P.L., Liu,Y., Jiricny,J., West,S.C. and Janscak,P. (2004) Human RECQ5beta, a protein with DNA helicase and strand-annealing activities in a single polypeptide. *EMBO J.*, **23**, 2882–2891.

60. Bugreev,D.V., Brosh,R.M. Jr. and Mazin,A.V. (2008) RECQ1 possesses DNA branch migration activity. *J. Biol. Chem.*, **283**, 20231–20242.

61. Cheok,C.F., Wu,L., Garcia,P.L., Janscak,P. and Hickson,I.D. (2005) The Bloom's syndrome helicase promotes the annealing of complementary single-stranded DNA. *Nucleic Acids Res.*, **33**, 3932–3941.

62. Machwe,A., Lozada,E.M., Xiao,L. and Orren,D.K. (2006) Competition between the DNA unwinding and strand pairing activities of the Werner and Bloom syndrome proteins. *BMC Mol. Biol.*, **7**, 1.

63. Macris,M.A., Krejci,L., Bussen,W., Shimamoto,A. and Sung,P. (2006) Biochemical characterization of the RECQ4 protein, mutated in Rothmund-Thomson syndrome. *DNA Repair*, **5**, 172–180.

64. Machwe,A., Xiao,L., Groden,J., Matson,S.W. and Orren,D.K. (2005) RecQ family members combine strand pairing and unwinding activities to catalyze strand exchange. *J. Biol. Chem.*, **280**, 23397–23407.